Research Repository UCD

Title	Phenotype-based Discovery of 2-[(E)-2-(Quinolin-2-yl)vinyl]phenol as a Novel Regulator of Ocular Angiogenesis
Authors(s)	Reynolds, Alison, Alvarez, Yolanda, Sasore, Temitope, Waghorne, Nora, Butler, Clare T., Kilty, Claire, Smith, Andrew J., Galvin, Orla, Merrigan, Stephanie, Grebnev, Gleb, Kennedy, Breandán, et al.
Publication date	2016-04-01
Publication information	Reynolds, Alison, Yolanda Alvarez, Temitope Sasore, Nora Waghorne, Clare T. Butler, Claire Kilty, Andrew J. Smith, et al. "Phenotype-Based Discovery of 2-[(E)-2-(Quinolin-2-Yl)Vinyl]Phenol as a Novel Regulator of Ocular Angiogenesis." American Society for Biochemistry and Molecular Biology, April 1, 2016. https://doi.org/10.1074/jbc.M115.710665.
Publisher	American Society for Biochemistry and Molecular Biology
Item record/more information	http://hdl.handle.net/10197/9315
Publisher's version (DOI)	10.1074/jbc.M115.710665

Downloaded 2026-05-01 00:54:59

The UCD community has made this article openly available. Please share how this access benefits you. Your story matters! (@ucd_oa)

© Some rights reserved. For more information

THE JOURNAL OF BIOLOGICAL CHEMISTRY VOL. 291, NO. 14, pp. 7242–7255, April 1, 2016
© 2016 by The American Society for Biochemistry and Molecular Biology, Inc. Published in the U.S.A.

Phenotype-based Discovery of 2-[(*E*)-2-(Quinolin-2-yl)vinyl]phenol as a Novel Regulator of Ocular Angiogenesis*

Received for publication, December 16, 2015, and in revised form, January 26, 2016 Published, JBC Papers in Press, February 4, 2016, DOI 10.1074/jbc.M115.710665

Alison L. Reynolds[‡], Yolanda Alvarez[‡], Temitope Sasore[‡], Nora Waghorne[‡], Clare T. Butler[‡], Claire Kilty[‡], Andrew J. Smith[‡], Carmel McVicar[§], Vickie H. Y. Wong[§], Orla Galvin[‡], Stephanie Merrigan[‡], Janina Osman[¶], Gleb Grebnev[‡], Anita Sjölander[¶], Alan W. Stitt[§], and Breandán N. Kennedy[‡1]

From the [‡]University College Dublin School of Biomolecular and Biomedical Science, Conway Institute, University College Dublin, Belfield, Dublin 4, Ireland, the [§]Centre for Experimental Medicine, Queen's University Belfast, Wellcome-Wolfson Building, 97 Lisburn Road, Belfast, BT9 7BL, United Kingdom, and the [¶]Division of Cell and Experimental Pathology, Department of Translational Medicine, Lund University, Skåne University Hospital, 20502 Malmö, Sweden

Retinal angiogenesis is tightly regulated to meet oxygenation and nutritional requirements. In diseases such as proliferative diabetic retinopathy and neovascular age-related macular degeneration, uncontrolled angiogenesis can lead to blindness. Our goal is to better understand the molecular processes controlling retinal angiogenesis and discover novel drugs that inhibit retinal neovascularization. Phenotype-based chemical screens were performed using the ChemBridge Diverset™ library and inhibition of hyaloid vessel angiogenesis in Tg(*fli1:EGFP*) zebrafish. 2-[(*E*)-2-(Quinolin-2-yl)vinyl]phenol, (quininib) robustly inhibits developmental angiogenesis at 4–10 μM in zebrafish and significantly inhibits angiogenic tubule formation in HMEC-1 cells, angiogenic sprouting in aortic ring explants, and retinal revascularization in oxygen-induced retinopathy mice. Quininib is well tolerated in zebrafish, human cell lines, and murine eyes. Profiling screens of 153 angiogenic and inflammatory targets revealed that quininib does not directly target VEGF receptors but antagonizes cysteinyl leukotriene receptors 1 and 2 ($CysLT_{1-2}$) at micromolar IC_{50} values. In summary, quininib is a novel anti-angiogenic small-molecule CysLT receptor antagonist. Quininib inhibits angiogenesis in a range of cell and tissue systems, revealing novel physiological roles for CysLT signaling. Quininib has potential as a novel therapeutic agent to treat ocular neovascular pathologies and may complement current anti-VEGF biological agents.

In the eye, developmental angiogenesis is a critical biological process enabling vision (1). Morphogenesis of the retinal vasculature is strictly controlled to balance high metabolic requirements while maintaining visual function. Uncontrolled pathological angiogenesis in the retina, choroid, and iris results in proliferative diabetic retinopathy, neovascular age-related macular degeneration, retinal vein occlusion, and retinopathy of prematurity, which are leading causes of blindness worldwide (2–5). Our understanding of the endogenous and exogenous factors regulating the overlapping but distinct phenotypes of developmental and pathological ocular angiogenesis is limited (6). Unbiased, phenotype-based chemical screens provide an opportunity to efficiently identify novel pharmacological inhibitors of angiogenesis in the eye (7, 8). These drugs and their molecular targets enhance our fundamental knowledge of the signaling networks regulating ocular angiogenesis and highlight alternative therapeutic interventions for angiogenesis-related disease.

An intricate balance of growth and inhibitory factors regulates angiogenesis (9). Imbalances can result in growth of abnormal, leaky vessels (6). Pathological angiogenesis is a hallmark of blinding ocular neovascular disease (3, 6), including neovascular age-related macular degeneration, which affects 2.6 million European Union and United States patients and whose prevalence is increasing because of an aging population (10, 11). Ocular neovascular disorders are regularly treated with biological agents (*e.g.* ranibizumab, bevacizumab, and aflibercept) targeting VEGF, a key proangiogenic mediator (12–14). Unfortunately, many patients do not respond clinically or become refractory to treatment (15). For example, ~46% of diabetic macular edema patients require additional laser treatment, and limited improvement in visual acuity is achieved (16). This, coupled with an undesirable intraocular delivery route, large clinical burden and expensive biological therapies highlight the need for improved ocular neovascular therapeutic agents (10).

The retina is a highly metabolically active tissue needing significant nourishment and oxygen supply (17). The adult retina in most mammals is nourished by two vascular networks. The choroid vessels overlying the retinal pigmented epithelium (RPE) nourish the outer retina. The inner retinal vessels at the ganglion cell layer develop at late embryonic stages and complete their morphogenesis after birth (1, 18). During development, the inner mammalian retina is nourished by the hyaloid vasculature, a transient capillary network located between the lens and retina. Later, hyaloid vessels undergo programmed regression, and a retinal vasculature forms by angiogenesis (1, 18, 19). Defects in hyaloid vasculature regression, known as persistent fetal vasculature, result in pathological eye conditions (20). In zebrafish, intraocular vasculature development is

* This work was supported by funding from an Enterprise Ireland proof of concept award, an Enterprise Ireland Commercialisation Fund award, a Health Research Board Ireland Health Research Award, and a Science Foundation Ireland Technology innovation development award. B. N. K. and Y. A. are authors on granted patent WO2012095836 A1. A. R., C. K., and B. N. K. are authors on patent filing WO2014012889 A1.

[1] To whom correspondence should be addressed: F062 UCD Conway Institute, UCD School of Biomolecular and Biomedical Science, Conway Institute, University College Dublin, Belfield, Dublin 4, Ireland. Tel.: 353-1-716-6740. E-mail: brendan.kennedy@ucd.ie.

initially similar to mammals. However, hyaloid vessels do not regress after embryonic development but progressively lose contact with the lens and, by 30 days after fertilization, adhere to the inner limiting membrane of the juvenile retina (21). In adult zebrafish, these vessels are found attached to the ganglion cell layer, exhibiting distinctive hallmarks of mammalian retinal vasculature (21, 22). Although the cellular morphogenesis of zebrafish hyaloid vasculature is well characterized, our understanding of the molecular regulators is limited to a small number of genetic and pharmacological studies (7, 8, 23).

Zebrafish are particularly amenable to phenotype-based drug discovery (24, 25). This "target-agnostic" approach focuses on a chosen phenotype and does not require prior selection of a molecular target. In this study, we identify unique drugs inhibiting developmental angiogenesis of the eye by performing an unbiased screen of ~1800 small-molecule drugs in the zebrafish hyaloid vessel assay (7). The screen uncovered 2-[(*E*)-2-(quinolin-2-yl)vinyl]phenol (quininib)[2] as a potent inhibitor of developmental angiogenesis in the zebrafish eye. Subsequently, quininib demonstrated significant anti-angiogenic activity in human endothelial cell, murine aortic ring, and murine oxygen-induced retinopathy models of angiogenesis. Target profiling identified quininib as a cysteinyl leukotriene 1 and 2 receptor ($CysLT_{1-2}$) antagonist. The cysteinyl leukotrienes LTC_4, LTD_4, LTE_4, and LTF_4 are bioactive lipids synthesized from cell membrane arachidonic acid via a 5-hydroxyeicosatetraenoic acid intermediate and signal via G protein-coupled receptors ($CysLT_1$, $CysLT_2$, GPR17, and GPR99) (26–30). $CysLT_1$ antagonists are commonly used to treat asthma and allergic rhinitis (31, 32). Previous studies have reported a role for CysLTs in inflammation, vascular permeability, immune responses, tissue repair, and regeneration (28, 33–36). $CysLT_2$ and $CysLT_1$ are expressed in the murine retina, and exogenous cysLTs are sufficient to induce retinal edema (37). Here quininib inhibits known cysteinyl leukotriene receptor signaling pathways, reducing ERK phosphorylation in response to leukotriene D4 agonism (38, 39). In summary, from unbiased chemical screens, we advance prior reports on cysLTs and demonstrate that a $CysLT_{1-2}$ antagonist significantly attenuates angiogenesis in the eye.

Experimental Procedures

Animal Use—Procedures were approved by the University College Dublin Animal Research Ethics Committee and performed under a Department of Health license and adhered to the Association for Research in Vision and Ophthalmology Statement for the Use of Animals in Ophthalmic and Visual Research. Wild-type C57BL/6J mice were obtained from Charles River Laboratories.

Phenotype-based Chemical Screens of Ocular Developmental Angiogenesis—ChemBridge DIVERSetTM library drug-like chemicals were screened (40). For all experiments, drugs were initially dissolved to 10 mM in DMSO and further diluted to the relevant concentration in double-distilled H_2O. Transgenic Tg[*fli1:EGFP*] zebrafish embryos (41) were drug-treated as reported previously (7). A compound was designated a primary hit when more than three of five treated larvae exhibited >50% reduced primary hyaloid vessels. Compounds confirmed in replicate experiments were designated secondary hits. Chemical analogues were identified using the ChemBridge hit 2 lead search engine. The MEK-1/2 inhibitor TAK-733 and the broad-spectrum PKC inhibitor Gö 6983 were purchased from SelleckChem.

Zebrafish Optokinetic Response Assay—The optokinetic response assay was performed on larvae treated from 2–5 days post-fertilization (dpf) and 3–5 dpf (7, 42). The drug was removed prior to the optokinetic response assay, and the larvae were washed in embryo medium. The average number of saccades/minute was manually quantified ($n = 30$ zebrafish/data point).

Intravitreal Murine Maximum Tolerated Dose—C57BL/6J mice aged 3– 6 months were anesthetized (ketamine, 67 mg/kg; medetomidine, 0.67 mg/kg), and 5-μl final concentrations of drug were injected intravitreally. Eyes were pierced below the pars planar using a 30-gauge needle, and the test drug was injected through this incision into the vitreous using a Nanofil syringe attached to a 33-gauge needle (World Precision Instruments). Post-injection, atipamezole (0.67 mg/kg) was administered. Mice were monitored and scored daily and culled 7 days after injection.

Histological Analysis of Zebrafish and Murine Eyes—Zebrafish larvae and mouse eyes were processed as reported previously (7). Mice were culled by carbon dioxide asphyxiation, and eyes were fixed in 2% paraformaldehyde/2.5% glutaraldehyde/0.1 M Sorenson's buffer. Prior to embedding, extraneous musculature was trimmed from the sclera and cornea, and the lens was removed, generating an eye cup that was bisected near the optic nerve. 500-nm sections were cut on a Leica EM UC6 microtome, stained with toluidine blue, and cover-slipped with DPX mounting medium. Sections from the central retina adjacent to the optic nerve were imaged and analyzed using NIS Elements BR on a Nikon E80i microscope.

Viability Assays in Human Cell Lines—3-(4,5-dimethylthiazol-2-yl)-2,5-diphenyltetrazolium bromide dye reduction assays were performed according to the protocol of the manufacturer to determine the viability of dermally derived human microvascular endothelial cells (HMEC-1) or human retinal pigment epithelium cells (ARPE-19), which were maintained as described previously (43).

In Vitro Tubule Formation in Human Microvascular Endothelial Cells—Microslide angiogenesis plates (IBIDI) were coated with Matrigel matrix (BD Biosciences), and tubule formation assays were performed according to the guidelines of the manufacturer. For all experiments, drugs were initially dissolved to 10 mM in DMSO and further diluted to the relevant concentration in MCDB 131 medium (Gibco). Total tubule length was quantified using Zeiss Axiovision image analysis software. Calcein AM stain (Invitrogen) 2 μg/ml was incubated with HMEC-1 cells following tubule formation for 30 min at 37 °C. Cells were imaged using brightfield and fluorescent microscopy.

[2] The abbreviations used are: quininib, 2-[(*E*)-2-(quinolin-2-yl)vinyl]phenol; CysLT, cysteinyl leukotriene; DMSO, dimethyl sulfoxide; OIR, oxygen-induced retinopathy; P12, postnatal day 12; ANOVA, analysis of variance; HV, hyaloid vessel; dpf, day(s) post-fertilization.

Anti-angiogenic Activity in an ex Vivo Mouse Aortic Ring Model—The aortic ring angiogenesis assay was performed according to an established protocol (44). For all experiments, drugs were initially dissolved to 10 mM in DMSO and further diluted to the relevant concentration in medium. Aortic rings were drug-treated in 150 μl of DMEM supplemented with 10% FCS and incubated at 37 °C/5% CO_2 for 6 days, when sprouts from the aortic ring perimeter were imaged using an Olympus CKX41 inverted phase-contrast microscope running ImageJ software and quantified as a percentage of vehicle control.

Mouse Ocular Angiogenesis Model—The mouse oxygen-induced retinopathy (OIR) model followed established protocols (45, 46). For all experiments, drugs were initially dissolved to 10 mM in DMSO and further diluted to the relevant concentration in Hanks' balanced salt solution. On postnatal day (P)12, each pup (>4 g) was administered oral acetaminophen (120 mg/5 ml) and anesthetized using ketamine (80 mg/kg) and medetomidine (0.67 mg/kg). Anesthetized pups were placed on heating pads and, using a Leica M651 ophthalmoscope, eyelids were opened by gently scoring with a beveled 30-gauge needle. A Dumont 7 forceps was used to gently proptose the eye, which was pierced just below the pars planar with a 33-gauge beveled needle attached to a Nanofil syringe (World Precision Instruments) angled behind the lens. 1 μl of drug or vehicle control was injected (rate of 1 μl/10 s), and the needle was left *in situ* for 60 s to allow pressure equilibration. Following intravitreal injection, atipamezole (0.67 mg/kg) was given. Uninjected controls were taken at P12 to confirm vascular regression. On P17, pups were culled by carbon dioxide asphyxiation, and the eyes were enucleated and fixed in 4% paraformaldehyde overnight at 4 °C.

Analysis of Murine Retinal Vascularization—Flat-mounted retinas were fluorescently stained with *Griffonia simplicifolia* isolectin (B4) and Alexa-streptavidin 568 as reported previously (47). Eyes were coverslipped using Aqua/Polymount and imaged using a Zeiss Axiovert 200 M fluorescent microscope running Andor IQ2 software and stitched using Andor montaging. Post-imaging, the total retinal area and total avascular area were measured using Fiji, and neovascular areas (measured from a 0.58 mm^2 area for each quadrant; neovascular tufts were precisely selected using the magnetic lasso tool) were measured using Imaris software. The avascular or neovascular area was expressed as a percentage of the total or defined retinal area, respectively. For vascular density analysis, a representative quadrant was selected from a subset of OIR samples ($n = 8–9$), and images were taken in 4-μm slices from the vitreal surface 0 μm (superficial) to 84 μm (deep retinal vascular bed) according to Sidman *et al.* (48). Statistical analysis was performed using one-way ANOVA with Dunnett's comparison post hoc test for multiple comparisons.

Target Profiling—10 μM quininib was screened for activity in the SelectScreen® Kinase Profiling Service (Invitrogen), which profiled 22 kinases, and the Premier Screen of 140 protein kinase targets (Dundee). The profiled kinases are reported in Fig. 5*A*.

Cysteinyl Leukotriene Receptor Assays—Drug antagonism was assessed in a guinea pig lung strip assay, where 3 nM LTD_4 was used to induce lung strip contraction. For cell-based assays, basal agonism or antagonism of 0.1 nM LTD_4-induced calcium mobilization was assessed in CHO-K1 cells overexpressing human $CysLT_1$, and 30 nM LTC_4-induced calcium mobilization was assessed in HEK 293 cells overexpressing human $CysLT_2$. For ligand-binding assays, the percentage of bound [^{3}H]LTD_4 in human recombinant CHO-K1 cells overexpressing $CysLT_1$ and human recombinant HEK 293 cells overexpressing $CysLT_2$ was quantified by scintillation counting.

$CysLT_{1–2}$ Expression Analyses—RNA was extracted from 3- and 5-dpf wild-type zebrafish eyes. The tissue was homogenized, and RNA was extracted using an RNeasy kit (Qiagen) and reverse-transcribed to cDNA using a Superscript III kit (Invitrogen). Primer sequences were as follows: zebrafish *cysltr1* (forward, 5-GGCATCTTGCGCACTCTACT; reverse, 5-GCAAAGCGTGATGACCACAG), zebrafish *cysltr2* (forward, 5-TGTTTGGAGCTCGCACATGA; reverse, 5-ATGATCACCAAAGCGCAAGC), and zebrafish *actb* (forward, 5-CGAGCAGGAGATGGGAACC; reverse, 5-CAACGGAAACGCTCATTGC).

Protein was extracted from human cell lines HMEC-1 (dermally derived endothelial cells), ACBRI-181 (primary retinal microvascular endothelial cells), and ARPE-19 (RPE cells). Cysteinyl leukotriene receptor expression was analyzed in immunoblots with primary antibodies (CysLT1R: Abcam, ab151484 (lot GR115651-4), 1:2000 with a goat anti-rabbit HRP-linked secondary antibody: Amersham Biosciences, NA934 (lot 9572648), 1:4000; CysLT2R: Santa Cruz Biotechnology, sc-27097 (lot F2514), 1:1000 with a donkey anti-goat IgG-HRP secondary antibody 1:2000 and α tubulin, Sigma, T9026, 1:10,000).

$CysLT_{1–2}$ Pathway Analysis—HMEC-1 cells were seeded at 2.5×10^5/well. After 24 h, the medium was changed, and cells were serum-starved for 24 h. Cells were stimulated with LTD_4 (10–1000 nM) for 5 min. For pathway inhibition studies, cells were pretreated with quininib or TAK-733 (10 μM) for 30 min, followed by 5-min stimulation with 500 nM LTD_4. Control cells were stimulated with 0.1% DMSO and 0.25% ethanol. After treatments, cells were washed with ice-cold PBS, harvested, and lysed with lysis buffer as described previously (43). Protein concentration was determined using the BCA protein assay kit (Pierce). For immunoblotting, an equal amount of protein (20 μg) was prepared in 5× sample buffer and separated by 10% SDS/PAGE, transferred to PVDF membranes (Sigma), and probed with primary and anti-rabbit or anti-mouse HRP-labeled secondary antibody (anti-mouse, Amersham Biosciences, NA934, lot 9572648). The primary antibodies used were phospho-p44/42 MAPK (Erk1/2, Cell Signaling Technology, 4370S, lot 15, 1:2000) and p44/42 MAPK (Erk1/2, Cell Signaling Technology, 9102S, lot 26, 1:1000) and α tubulin (1:10,000). Chemiluminescent detection using Amersham Biosciences ECL Prime detection reagent (GE Healthcare, RPN2232) allowed visualization of protein. Quantitative measurement of the phosphorylated protein level was performed using ImageJ. Results are presented as relative densitometry ratios of phosphoprotein relative to the band intensity of total protein.

Results

Phenotype-based Screens in Zebrafish Uncover Novel Anti-angiogenic Compounds—In an unbiased anti-angiogenic drug discovery approach, 1760 randomized small-molecule compounds from the ChemBridge DiverSET™ library were

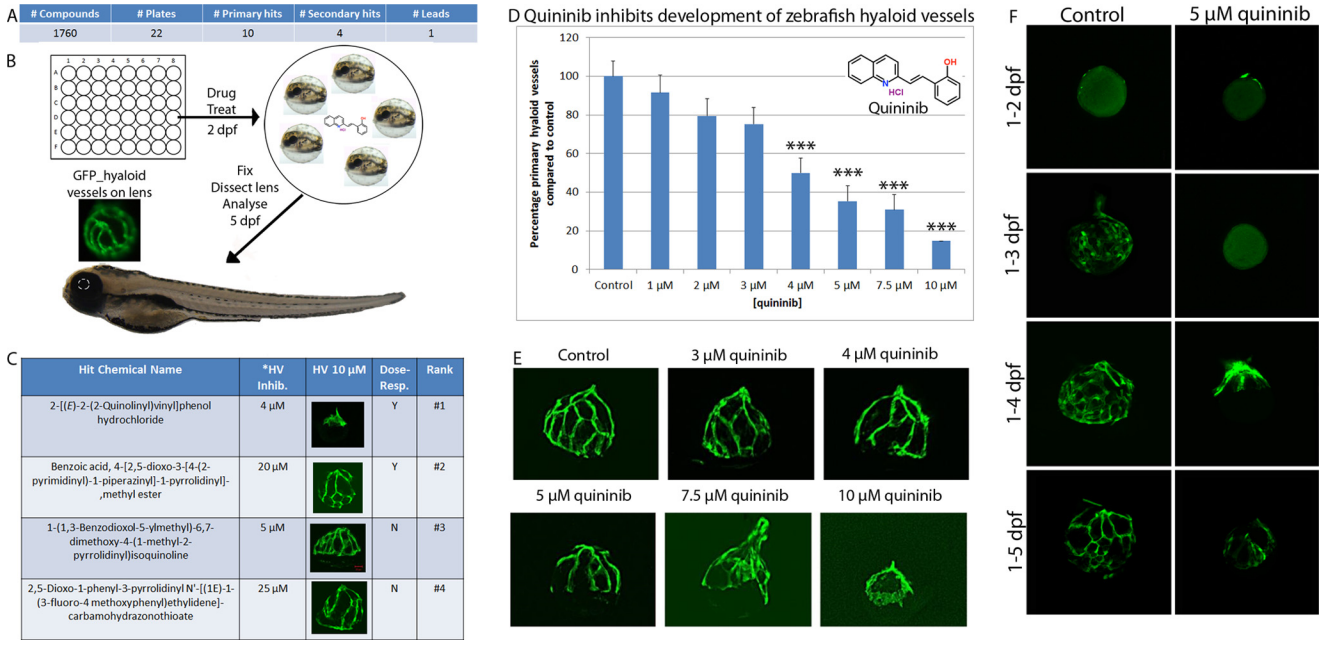

FIGURE 1. **Hit quininib was identified in chemical screens of ocular developmental angiogenesis.** 1760 compounds from the ChemBridge DiverSET™ library (*A*) were tested for the ability to attenuate developmental angiogenesis of zebrafish hyaloid vasculature (*B*). Ten primary hits were identified (>50% reduction in primary hyaloid vessels in three or more of five treated larvae), and four were selected for validation (*C*, the *asterisk* refers to the minimum effective dose). Quininib ranked highest on the basis of robust, reproducible anti-angiogenic activity at multiple doses (*C*). Quininib (*D*, *inset*) generates a dose-dependent, significant inhibition of the number (mean ± S.E.) of primary hyaloid vessels that develop ($n = 10$ zebrafish/dose). The number of primary hyaloid vessels is quantified and graphed as a percentage of control, which has an average of 3.4 primary vessels (*D*). Representative images of hyaloid vasculature formation on dissected zebrafish lenses (*E*) qualitatively demonstrate the anti-angiogenic activity of quininib on the entire hyaloid vasculature. Representative images from a time-course treatment carried out from 1–2, 3, 4, or 5 dpf (*F*) demonstrated that 5 μM quininib abolished and then delayed vessel sprouting. Statistics were performed using one-way ANOVA (with Dunnett's post hoc correction). ***, $p < 0.001$.

screened in larval zebrafish (Fig. 1, *A* and *B*). Anti-angiogenic activity was quantified on the basis of the ability of 10 μM of each compound to significantly inhibit developmental angiogenesis of the primary hyaloid vessels (HVs) in the eye of TG[*fli1:EGFP*] larvae (21). Ten primary hits were identified on the basis of the criterion of >50% HV inhibition in >60% larvae. Of these, four secondary hits inhibited primary branch HV development in replicate experiments, a hit rate of 0.23% (Figs. 1, *A–C*, and 2). Dose-response experiments determined that quininib (CAS no. 1379458-56-6; Fig. 1*D*, *inset*) ranked with the highest efficacy and potency, inhibiting primary HV development by 85% with an IC_{50} of ~4 μM (Fig. 1*D*). Quininib exerted a dose-dependent inhibition on the number of primary HVs (Fig. 1*D*), and fluorescent images of dissected lenses demonstrated quininib to robustly stunt growth of the entire basket-shaped hyaloid vasculature (Fig. 1*E*). Time-course analyses that looked at the effect of quininib on the initial formation of hyaloid vasculature at 2, 3, 4, and 5 dpf demonstrated that quininib initially completely abrogated primary vessel sprouting. Delayed primary vessels appeared at 4 dpf, but the branching pattern at 5 dpf was visibly reduced compared with vehicle controls at 3 dpf. Cell density appeared normal in the quininib-treated drug vessels (Fig. 1*F*).

A Structural Analogue of Quininib Significantly Inhibits HV Development—To corroborate the specific pharmacological response produced by quininib, commercial analogues were assayed for anti-angiogenic activity. 4-Bromo-2-(2-quinolin-2-yl-vinyl)-phenol (QB-590, CAS no. 337352-14-4) had inclusion of a 5-bromo substituent. (4-[(*E*)-2-Vinyl]phenol (QB-663, CAS no. 430459-22-6) changed the hydroxy group to the 4′ from the 2′ position and inclusion of an ester linkage at C-8. QB-771 changed the hydroxy group to the 4′ from the 2′ position and included a 6′-bromo substituent and an ester linkage at C-3′. 4-bromo-2-(2-quinolin-2-yl-vinyl)-phenol, 4-[(*E*)-2-vinyl]phenol, and QB-771 did not exhibit biological activity in the HV assay (Fig. 3). However, the quininib Z-isomer and the other most structurally related analogue, 4-[(*Z*)-2-(4-quinolinyl)vinyl]phenol (QB-799, CAS no. 1379458-54-4), which contains a Z-isomer configuration and relocation of the phenol ring hydroxy group to the 4′ position, phenocopied quininib and reduced primary zebrafish HV development by ~34% (Fig. 3).

Safety Pharmacology—Quininib is well tolerated at concentrations that elicit anti-angiogenic responses (Fig. 4). 2- 5-dpf zebrafish treated with 10 μM quininib developed normally, except for some pericardial edema, hypopigmentation, and reduced eye size (Fig. 4*A*). In addition, treatment of zebrafish larvae with 10 μM quininib from 2–5 dpf did not affect the existing intersegmental vasculature but did affect formation of the subintestinal vessels (which form after 2.5 dpf), suggesting that quininib preferentially inhibits newly forming vessels (Fig. 4, *B* and *C*). Quininib-treated zebrafish eyes have equivalent ocular histology to vehicle controls, with comparable central retinal morphology, diameter, lamination, RPE pigmentation, and absence of pyknotic nuclei (Fig. 4*E*). In contrast, zebrafish visual behavior was significantly or moderately reduced with 10 or 5 μM quininib, respectively (Fig. 4*D*). In human cell lines, <25 μM quininib was well tolerated for 96 h in retinal pigment

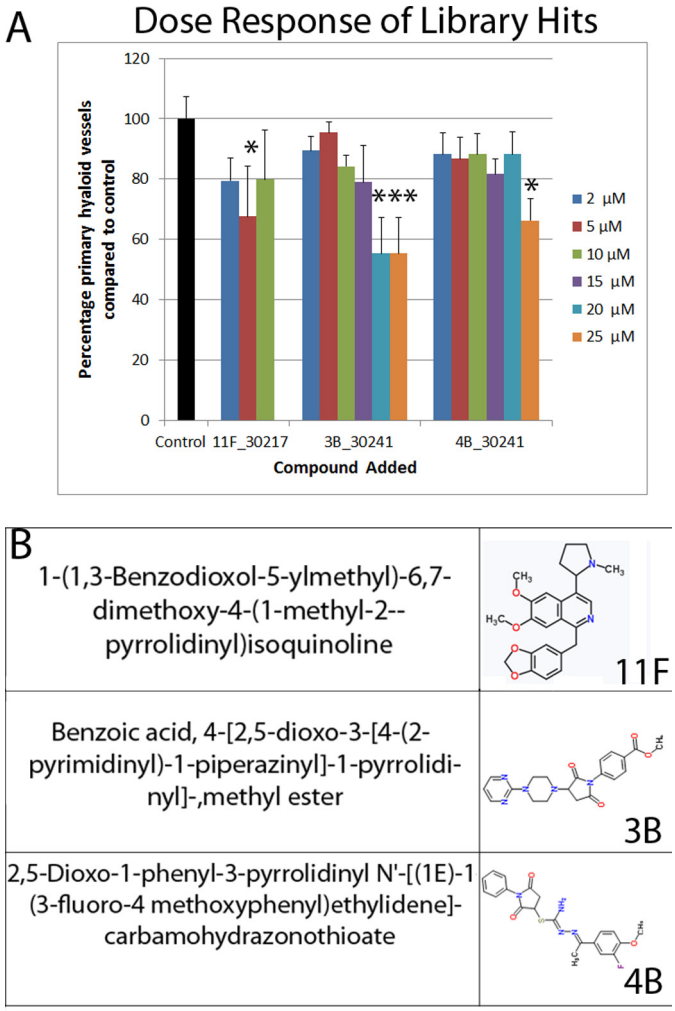

FIGURE 2. **Dose-response activity of selected screen hits 11F, 3B, and 4B.** Compounds 11F, 3B, and 4B showed efficacy at 10 μM on the basis of the initial screen criteria but not in validation experiments, wherein the average reduction in primary HV is graphed (*A*). 11F and 4B do not demonstrate a dose-dependent anti-angiogenic activity. 11F only demonstrated inhibition at 5 μM, whereas the minimal effective doses of 3B and 4B were 20 and 25 μM, respectively (n = 5–10 zebrafish/dose). These compounds were not progressed further. The number of primary hyaloid vessels is quantified and graphed as a percentage of control, which has an average of 3.4 primary vessels. Data shown are mean ± S.E. Statistics were performed using one-way ANOVA (with Dunnett's post hoc correction). *, $p < 0.05$; ***, $p < 0.001$. The chemical names and two-dimensional structures of 11F, 3B, and 4B are given in *B*.

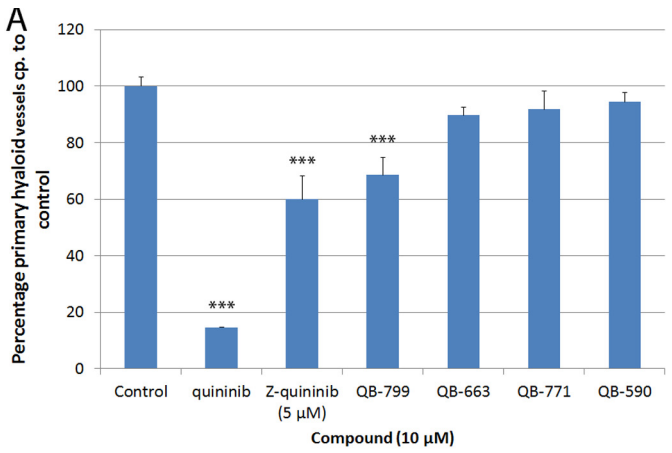

B		
Z-quininib	2-[(*Z*)-2-(2-Quinolinyl)vinyl]phenol hydrochloric acid salt	
QB-799	4-[2-(4-quinolinyl)vinyl]phenol	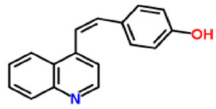
QB-663	4-[(*E*)-2-{8-[(2-Chlorobenzyl)oxy]-2-quinolinyl}vinyl]phenol	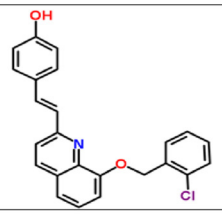
QB-771	5-bromo-2-ethoxy-4-[2-(8-methoxy-2-quinolinyl)vinyl]phenol	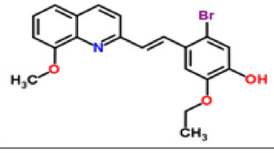
QB-590	4-Bromo-2-(2-quinolin-2-yl-vinyl)-phenol	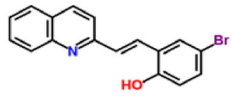

FIGURE 3. **Quininib analogs can inhibit ocular developmental angiogenesis in zebrafish.** Commercially available quininib analogues were tested in the zebrafish hyaloid vasculature assay. Two Z conformation analogues, Z-quininib and 4-[(*Z*)-2-(4-quinolinyl)vinyl]phenol, at 5 and 10 μM respectively, exhibited significant inhibition of ocular developmental angiogenesis, whereas three analogues were inactive (*A*). The number of primary hyaloid vessels is quantified and graphed as a percentage of control, which has an average of 3.4 primary vessels. The chemical names and two-dimensional structures of five tested analogues are shown in *B*. Data are given as mean ± S.E. Statistics were performed using one-way ANOVA (with Dunnett's post hoc test). ***, p <0.001 (n = 10 zebrafish/compound).

epithelium cells (ARPE-19) and 24 h in human microvascular endothelial cells (HMEC-1) (Fig. 4*F*). In contrast, 5–20 μM quininib reduced HMEC-1 viability by 20–30% at 96 h, consistent with an anti-angiogenic profile (Fig. 4*F*). In mice, intravitreally administered quininib had a maximum tolerated dose of 200 μM on the basis of ocular morphology. (Fig. 4*G*). Gross ocular morphology was unaffected. No cataracts, inflammation, or infections occurred up to 7 day post-delivery. Retinal histology was equivocal to controls with respect to retinal cell types, cell numbers, lamination, RPE pigmentation, and absence of pyknotic nuclei (Fig. 4*G*).

Target Profiling and CysLT$_1$ Antagonism—To elucidate the molecular mechanism of action of quininib, literature searches and target profile assays were undertaken. Previously, quininib was reported as a weak cysteinyl leukotriene 1 receptor (CysLT$_1$) antagonist (inhibited binding of [^{3}H]LTD$_4$ to guinea pig lung membrane, IC$_{50}$, >50 μM) and an endothelin-converting enzyme 2 inhibitor (IC$_{50}$, 6.42 μM) (49–51). Here target profiling of 153 putative targets revealed that only CysLT$_1$ was inhibited more than the 50% threshold criterion by 10 μM quininib (Fig. 5*A*). Of note, quininib did not significantly inhibit human endothelin-converting enzyme (ECE-1) or any of the human vascular endothelial growth factor recep-

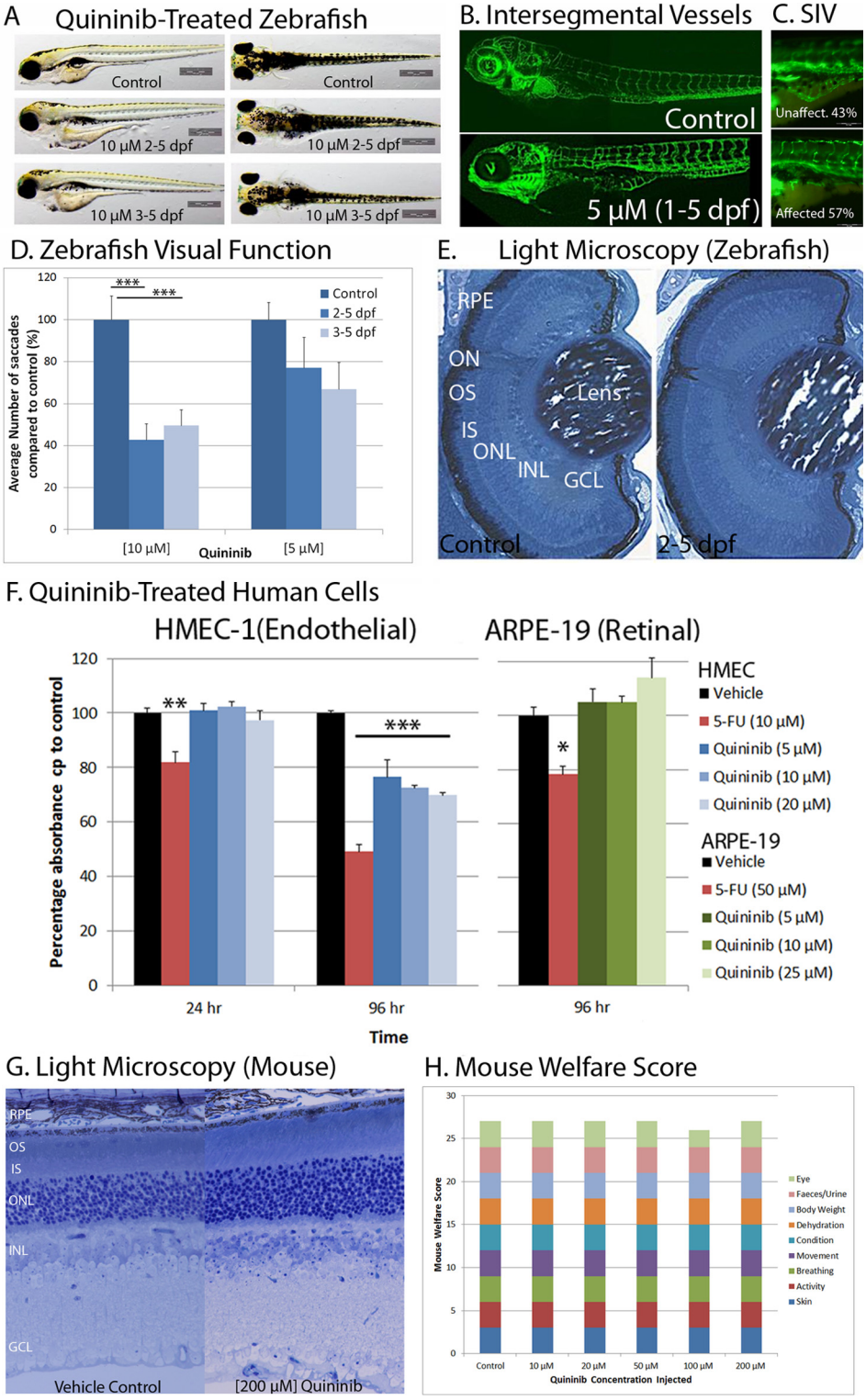

FIGURE 4. **Quininib is safe and well tolerated in zebrafish, human cell lines, and mouse retina.** *A*, dorsal and lateral images of zebrafish treated with 10 μM quininib from 2–5 dpf showing normal gross morphology with the exception of some pericardial edema, a marginally smaller eye diameter, and a slight reduction in pigmentation. Quininib treatment from 2–5 dpf showed no disruption of established vasculature, as exemplified by intact intersegmental vessels, which formed before 1 dpf (*B*), but did inhibit formation of the subintestinal vessels (*SIV*) formed from 2–5 dpf (*C*). 5 and 10 μM quininib reduced visual behavior ($n = 3$ replicates, 10 zebrafish/replicate) recorded from the optokinetic response (*D*). Light microscopy showed normal retinal morphology, including the presence of expected cell types, proper lamination, and lack of pyknotic nuclei in 2- 5-dpf quininib-treated larvae (*E*). 3-(4,5-dimethylthiazol-2-yl)-2,5-diphenyltetrazolium bromide cell viability assays showed that quininib is well tolerated at 20 μM for 24 h in a human endothelial cell line ($n = 3$) and at 25 μM for 96 h in a human retinal pigment epithelium cell line ($n = 1, 4$ replicates) (*F*). The quininib intravitreal maximum tolerated dose was determined in mouse eyes (*G* and *H*). Light microscopy (×40) of the central retina (near the optic nerve) showed a normal retinal morphology in 200 μM quininib-injected eyes: the presence of all cell types, similar thickness of layers, normal lamination, and lack of pyknotic nuclei (*G*). Mice were scored on a daily basis (for 7 days after injection) for nine general welfare traits. A score of 3 was normal. All scores were normal, with the exception of one mouse at 100 μM that had a corneal bleed visible 1 day after injection (*H*) ($n = 3$ mice/dose). *ON*, optic nerve; *OS*, outer segment; *IS*, inner segment; *ONL*, outer nuclear layer; *INL*, inner nuclear layer; *GCL*, ganglion cell layer.

A. Target Profiling

Target	% Inhib	Target	% Inhib	Target	% Inhib	Target	% Inhib	Target	% Inhib	Target	% Inhib	Target	%	Target	%	Target	%
CysLT1R	107	IKKe	24	STK3	16	MARK3	11	MELK	7	TAO1	2	DDR2	-2	TGFBR	-5	PIK3C2	-10
PLK	41	CLK2	23	VEGFR2	16	PAK6	10	IKKb	7	PDK1	2	FGFR1	-2	PKBa	-5	TLK1	-10
MLK	42	CSNK2A1	22	Lck	16	AMPK	10	CDK9	6	MKK6	2	PRK2	-2	JNK2	-6	RSK2	-10
HIPK2	34	MAP4K5	22	RIPK2	15	CHK2	9	CK1γ2	6	PKCa	2	Aurora	-2	MAPKA	-6	EPHB4	-11
PDGFRα	33.75*	MINK	21	IR	15	SGK1	9	IRAK1	5	CHK1	1	CK1δ	-2	CAMK	-6	ULK2	-11
PIM3	31	NTRK1	21	PKBb	14	TBK1	9	ULK1	5	MARK4	1	HIPK3	-2	PIM2	-6	MEKK1	-12
MLK1	30	SIK3	21	SIK2	14	PDGFRA	9	BRSK2	5	EPHB3	1	PHK	-3	EIF2AK	-6	ERK2	-13
SmMLCK	30	DYRK1A	21	DYRK3	14	TESK1	8	p38bMAPK	5	BRK	0	GSK3b	-3	HIPK1	-6	JNK1	-14
GCK	30	ECE1	20	CAMK1	13	PKD1	8	RSK1	4	TSSK1	0	PIK3C3	-3	PAK4	-7	NEK6	-15
TAK1	29	MAPKAPK3	20	AKT3	13	STK33	8	ROCK 2	4	p38aMAPK	0	SPHK1	-3	TTBK2	-7	YES1	-17
AURKB	28	EPHA2	20	Src	12	MARK2	8	PKCγ	4	p38gMAPK	0	SYK	-4	PAK2	-7	ABL	-18
PIK3CD	27	JAK2	19	EPHB1	12	ASK1	8	CDK2	4	MSK1	0	TTBK1	-4	EPHA4	-7	MKK1	-19
VEGFR1	16*	EF2K	19	MAP4K3	12	OSR1	7	NEK2a	4	MNK1	0	PKA	-4	BTK	-7	P14K4	-25
JNK3	26	PAK5	17	MAPK9	12	MST4	7	MPSK1	3	WNK1	0	AMPK	-4	PIK3CA	-8	PIK4B	-25
IRR	26	MAP2K5	17	BMX	11	SRPK1	7	PKCz	3	S6K1	-1	IGF1R	-4	p38dM	-8	IRAK4	-27
MAPKAPK5	25	MAPK15	16	MST3	11	MNK2	7	LKB1	3	EPHB2	-1	PIK3C2	-5	HER4	-8	ERK1	-28
NUAK1	25	PIM1	16	MKK2	11	BRSK1	7	VEGFR3	3	EGFR	-1	MARK1	-5	TIE2	-9	PIK3CG	-39

B. Representative IC50 Curves

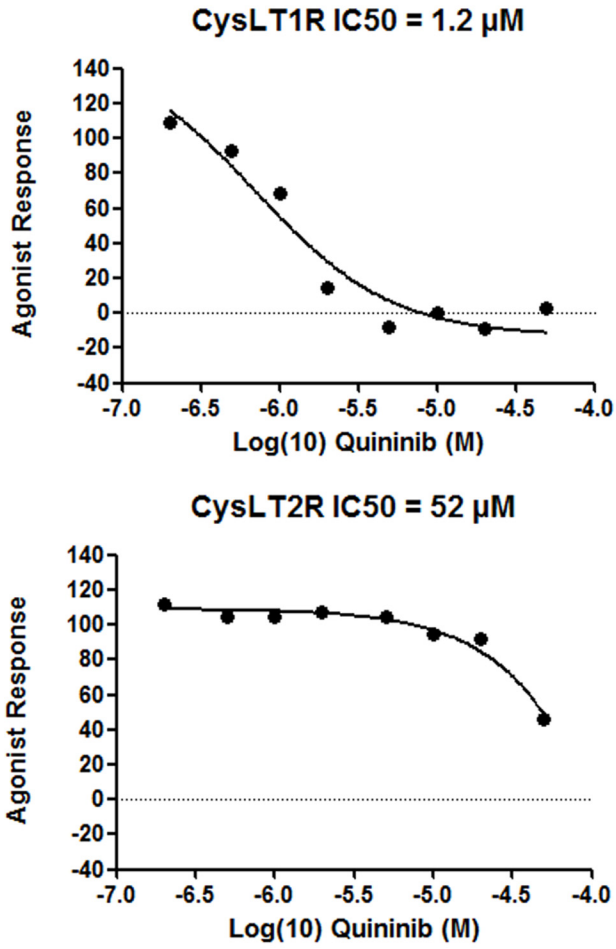

C. Cysteinyl Leukotriene Assays

Assay	Agonist	Competitor	% Antagonism
Guinea Pig Lung Strip Contraction	LTD_4	**Quininib (30 μM)**	**51%**
		Montelukast (30 μM)	89%
rCYSLTR1 Cell-Reporter Activation	LTD_4	**Quininib (10 μM)**	**107%**
rCYSLTR2 Cell-Reporter Activation	LTC_4	Quininib (10 μM)	18%
rCYSLTR1 Radioligand Binding	[^{3}H] LTD_4	**Quininib (10 μM)**	**65%**
rCYSLTR2 Radioligand Binding	[^{3}H] LTD_4	Quininib (10 μM)	2%

D. RNA Expression

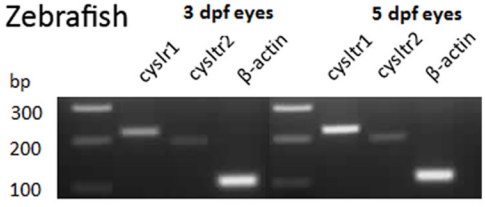

E. Protein Expression in Human Cells

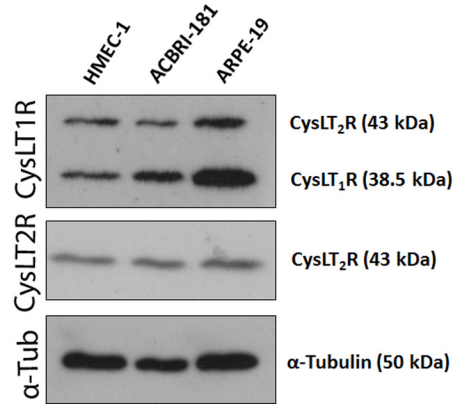

FIGURE 5. **Quininib is a cysteinyl leukotriene receptor 1 antagonist with an IC_{50} of 1.4 μM.** Target profiling of 153 targets with 10 μM quininib (*A*) identified activity in the cysteinyl leukotriene pathway. Quininib blocked 0.1 nM LTD_4-induced intracellular calcium release in CHO-K1 cells overexpressing $CysLT_1$ with an average IC_{50} of 1.4 μM (three replicates). Plotted is the non-linear regression curve for a representative experiment (*B*, *top panel*). Quininib also acted as a very weak $CysLT_2$ antagonist with an average IC_{50} of >38.5 μM (three replicates). Shown is the non-linear regression curve of a representative experiment (*B*, *bottom panel*). Upon further investigation, quininib appeared to act as an orthosteric $CysLT_1$ antagonist, blocking 50% of LTD_4-induced contraction in an *ex vivo* guinea pig lung strip assay (*C*) but exhibiting no agonist response (data not shown) and competing directly with the radiolabeled native agonist (LTD_4). The genes encoding $cysLT_1R$ and $cysLT_2R$ were expressed in zebrafish at 3 and 5 dpf (*D*). Both $CYSLT_1R$ and $CYSLT_2R$ were expressed in a human dermally derived endothelial cell line (HMEC-1), a human retinal microvascular endothelial cell line (ACBRI-181), and a human retinal pigment epithelial cell line. *E*, Western blotting analysis showing the expression of cysteinyl leukotriene receptors 1 and 2 and α-tubulin in three human cell lines. Note that the antibody for $CYSLT_1R$ also binds to $CYSLT_2R$ protein. For CysLT1R, PDGFRα, and VEGFR1, target profiling was performed in triplicate to confirm results (10 μM quininib inhibited intracellular calcium release by 107% ± 8% (below baseline) in CHO-K1 cells overexpressing $CysLT_1$, PDGFRα by 34% ± 13%, and VEGFR1 by 16% ± 18%. A hit was considered to inhibit >50% of the response).

tors (VEGFR1–3) that are clinically targeted in neovascular disease (Fig. 5, *A–C*).

Quininib Significantly Attenuates Angiogenesis in Mammalian Models—To determine whether quininib has an evolutionarily conserved anti-angiogenic bioactivity, it was tested in human and mouse models. In HMEC-1 cells, 3.16 μM quininib significantly inhibited (~44.2%) *in vitro* endothelial cell tubule formation (Fig. 6, *A* and *B*). In the *ex vivo* mouse aortic ring assay of angiogenesis, 10 μM quininib administered for 6 days significantly inhibited (35.9% ± 13%) sprout formation compared with vehicle controls (Fig. 6, *C* and *D*). To assess whether quininib inhibited ocular angiogenesis *in vivo*, the murine OIR model was utilized. Quininib was injected once intravitreally at the P12 transition from hyperoxia to normoxia (relative hypoxia), and analyses at P17 demonstrated inhibition of retinal revascularization (normal intraretinal vessel regrowth similar to developmental angiogenesis; Fig. 6, *E* and *F*) and, at higher quininib concentrations, increased retinal neovascularization (preretinal pathological neovascularization; Fig. 6, *G–I*). Compared with vehicle-injected controls, there was a 1.5-fold increase in avascular area in quininib-treated eyes (25%) *versus* vehicle-injected controls (16%) (Fig. 6, *E* and *F*). 0.5 μM quininib had no effect on neovascularization, whereas 3 μM quininib resulted in an increased neovascular area compared with vehicle controls (Fig. 6*G*). Relative vascular density analysis showed that, at P17, the retinal blood vessels were mainly found in the superficial layer and that vascular density was increased in 3 μM quininib-injected mice, reflecting the increase in neovascularization (Fig. 6, *H* and *I*).

$CysLT_1$ Antagonism—$CysLT_1$ was corroborated as a relevant target of quininib by competitive antagonist binding and activity assays and target expression profiling (Fig. 5, *B–E*). In guinea pig lung strip contraction assays, 30 μM quininib alone did not act as an agonist (data not shown). However, 30 μM quininib antagonized LTD_4-induced contraction by 51% (Fig. 5*C*). In radio-ligand binding assays, 10 μM quininib inhibited binding of [^{3}H]LTD4 to $CysLT_1$ and $CysLT_2$ by 65% and 15%, respectively (Fig. 5*C*). Cell-based assays of $CysLT_1$ or $CysLT_2$ activity confirmed that quininib preferentially antagonized the LTD_4-induced reporter activity of human $CysLT_1$ (IC_{50}, 1.4 μM; E_{max}, 137%) compared with $CysLT_2$ (IC_{50}, 38.5 μM; E_{max}, 45%) (Fig. 5*B*). Previous studies have confirmed retinal expression of $CysLT_1$ in rodent models of retinal neovascularization (37), and we demonstrated here ocular expression of the zebrafish *cysltr1* and *cysltr2* genes during hyaloid vessel development (Fig. 5*D*) and expression of cysteinyl leukotriene receptors 1 and 2 in human endothelial cells (HMEC-1), human retinal microvascular endothelial cells (ACBRI-181), and human RPE cells (ARPE-19) (Fig. 5*E*).

Other established $CysLT_1$ antagonists are clinically used for the treatment of upper and lower respiratory tract disorders (31, 32). A commonly prescribed $CysLT_1$ antagonist is montelukast (15)-3-[2-(2-hydroxy-2-propanyl) phenyl]propyl{sulfanyl)methyl]cyclopropyl}acetic acid. Montelukast is less effective than quininib at attenuating hyaloid vasculature development in zebrafish eyes. 20 μM montelukast is required to produce a significant reduction (15% fewer hyaloid vessels) *versus* 4 μM quininib (~50% fewer hyaloid vessels) (Fig. 1*D*, data not shown). In contrast, 30 μM montelukast was more effective than 30 μM quininib at antagonizing LTD_4-induced guinea pig lung strip contraction (89% *versus* 51%), and 10 μM montelukast or quininib reduced mouse aortic ring angiogenesis by an equivalent ~40% (Fig. 6, *C* and *D*). Interestingly, 0.5 μM quininib significantly attenuated revascularization in the OIR model, whereas 0.5 μM montelukast had a negligible effect (Fig. 6*E*). In summary, $CysLT_1$ antagonists can reduce angiogenesis, but, in the eye, quininib is significantly more effective than montelukast at attenuating ocular angiogenesis or revascularization in zebrafish and mice.

Downstream Inhibitors in the Cysteinyl Leukotriene Pathway Phenocopy Quininib—Downstream inhibitors of the cysteinyl leukotriene pathway (Fig. 7*A*) were tested to see whether they inhibited developmental angiogenesis in zebrafish. Drug treatment with the broad-spectrum PKC inhibitor Gö 6983 (10 μM) or the MEK 1/2 inhibitor TAK-733 (10 μM) inhibited the formation of primary hyaloid vessels in zebrafish (Fig. 7, *B–E*) by 43% and 38%, respectively, phenocopying quininib.

Quininib Affects $CysLT_{1-2}$ Signaling—HMEC-1 endothelial cells exhibit an up-regulation of cysteinyl leukotriene signaling pathways, as evidenced by an increase in phospho-ERK 44/42 expression, when stimulated with 10, 100, or 1000 nM LTD_4 for 5 min (Fig. 7*F*). Leukotriene D4-induced phospho-ERK 44/42 up-regulation is inhibited in the presence of quininib and the downstream MEK 1/2 inhibitor TAK-733 (Fig. 7*G*). Western blotting analyses show that quininib inhibits LTD_4-induced phospho-ERK 44/42 up-regulation by 29% compared with vehicle control (0.1% DMSO and 0.25% ethanol) (Fig. 7*H*). This is in comparison with the MEK 1/2 inhibitor TAK-733, which completely abolishes phospho-ERK expression with or without the presence of LTD_4.

Discussion

From phenotype-based screens of a randomized small molecule library, quininib was uncovered as a novel, robust inhibitor of angiogenesis *in vivo*. Quininib is an orthosteric cysteinyl leukotriene receptor 1 antagonist and a weak cysteinyl leukotriene receptor 2 antagonist. Overall, this research enhanced our understanding of the molecular pathways controlling ocular angiogenesis and identified drugs and molecular targets with potential to be developed into therapeutic agents for angiogenesis-related diseases.

Two studies previously identified inhibitors of zebrafish hyaloid vasculature development using phenotype-based chemical screens. Alvarez *et al.* (7) identified LY 294,002, a PI3K inhibitor, in a screen of 11 known angiogenic modulators. In a screen of ~2000 bioactive drugs from the MicroSource Spectrum collection, Kitambi *et al.* (8) identified pyrogallin, an ATP-competitive inhibitor of JAK3, plus albendazole and mebendazole, both anti-helminthic medications that inhibit microtubule assembly. Thus, both studies screened existing bioactive compounds. Our study differs in that a randomized library (ChemBridge DiverSET^{TM}) of ~1800 molecules with predicted drug-like physiochemical properties was screened with the intent of identifying novel regulators of developmental angiogenesis in the eye.

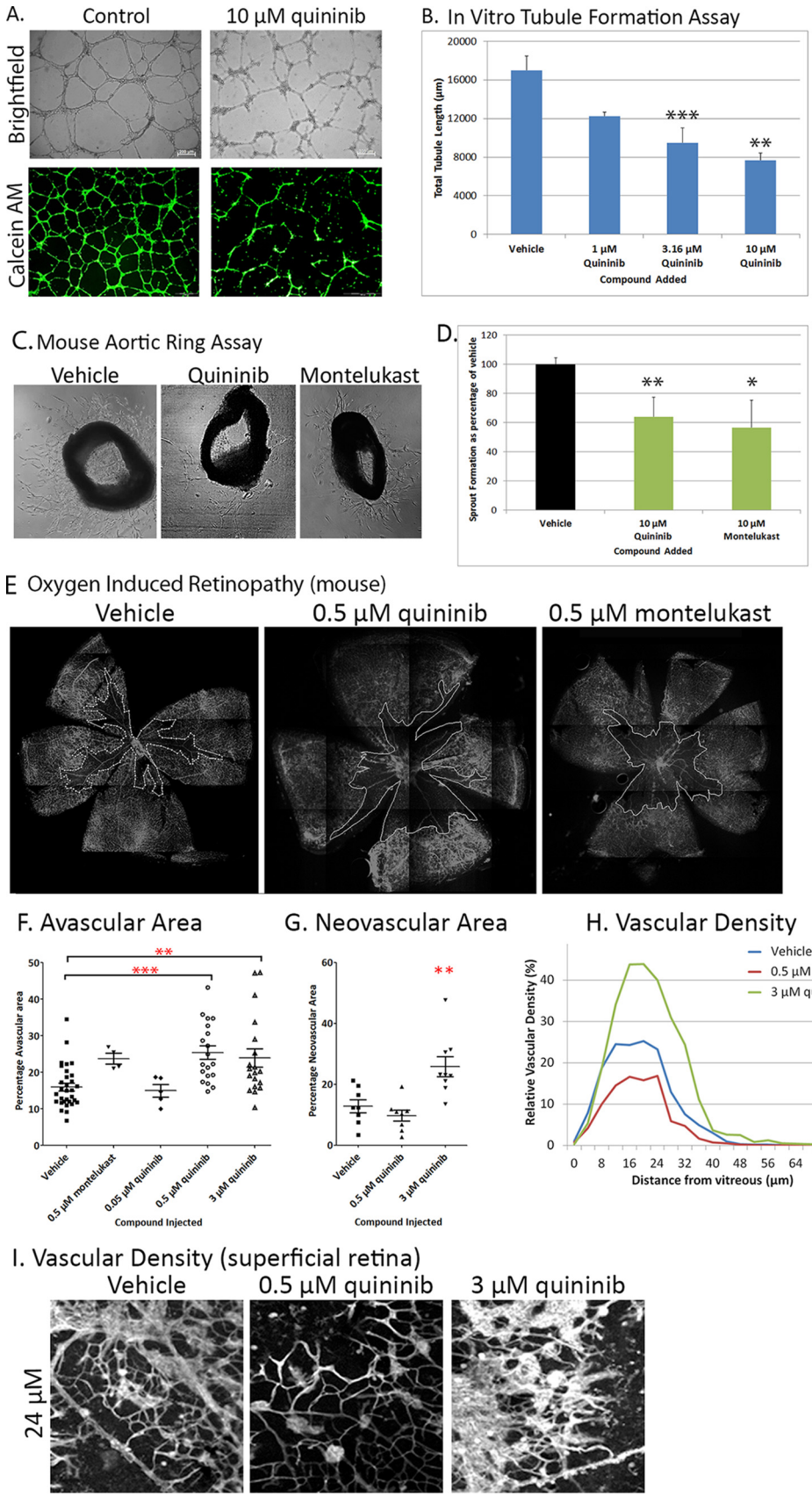
A.
Control
10 µM quininib
Brightfield
Calcein AM
B. In Vitro Tubule Formation Assay
Total Tubule Length (µm)
20000
16000
12000
8000
4000
0
***
**
Vehicle
1 µM Quininib
3.16 µM Quininib
10 µM Quininib
Compound Added
C. Mouse Aortic Ring Assay
Vehicle
Quininib
Montelukast
D.
Sprout Formation as percentage of vehicle
120
100
80
60
40
20
0
**
*
Vehicle
10 µM Quininib
10 µM Montelukast
Compound Added
E Oxygen Induced Retinopathy (mouse)
Vehicle
0.5 µM quininib
0.5 µM montelukast
F. Avascular Area
Percentage Avascular area
50
40
30
20
10
0
**
***
Vehicle
0.5 µM montelukast
0.05 µM quininib
0.5 µM quininib
3 µM quininib
Compound Injected
G. Neovascular Area
Percentage Neovascular Area
60
40
20
0
**
Vehicle
0.5 µM quininib
3 µM quininib
Compound Injected
H. Vascular Density
Vehicle
0.5 µM quininib
3 µM quininib
Relative Vascular Density (%)
40
30
20
10
0
0 8 16 24 32 40 48 56 64 72 84
Distance from vitreous (µm)
I. Vascular Density (superficial retina)
Vehicle
0.5 µM quininib
3 µM quininib
24 µM

Analysis in zebrafish, human, and rodent models demonstrates that quininib is an effective and well tolerated inhibitor of angiogenesis. Efficacy in the zebrafish model upon administration into the larval medium confirms desirable *in vivo* pharmacokinetic properties that support bioavailability beyond effective threshold concentrations in ocular tissue. Quininib inhibits the formation of newly forming but not existing vessels and so fits the properties of a vascular targeting agent and not a vascular disrupting agent (52). The anti-angiogenic effect of quininib is a specific pharmacological response and cannot be attributed to toxic effects or developmental delay in the models investigated. Quininib-treated larvae, however, present with a defective optokinetic response. In agreement, previous genetic studies report that zebrafish lacking ocular vasculature (*cloche* and *silent heart* mutants or VEGF-A morphants) exhibit reduced differentiation of retinal neurons and impaired synaptic processes (53, 54). The reduced visual behavior of quininib-treated zebrafish larvae is not an overt concern for further drug development because it likely reflects an indirect developmental defect that would not be encountered in adult eyes.

In mammalian models, quininib is well tolerated in mice and is effective at inhibiting angiogenesis in the mouse oxygen-induced retinopathy model of ocular angiogenesis via an intravitreal delivery route. Two phases of blood vessel growth occur following the relative hypoxia that occurs when these mice are returned to normoxia on P12. These phases are a revascularization (normal intraretinal vessel regrowth), which is similar to a recapitulation of developmental angiogenesis, and a preretinal pathological neovascularization (55). Both 0.5 and 3 μM quininib are effective at blocking retinal revascularization in the OIR model, with equivalent responses observed with 0.5 and 3 μM quininib, suggesting attainment of a maximum response plateau. Curiously, neovascularization in drug-treated eyes shows that the lower quininib dose slightly reduces neovascularization, whereas the higher dose increases the relative neovascular area. This may be due to the drug targeting one specific CysLT receptor at lower concentrations and more than one CysLT receptor at higher concentrations. In agreement, Barajas-Espinosa *et al.* (37) reported a similar finding when *Cyslt2r* knockout mice were exposed to the OIR experimental paradigm. P17 flat-mount retinas, the same time point analyzed in our study, exhibited both reduced revascularization and increased neovascularization. They postulated that the increased neovascularization is due to the compensatory up-regulation of $CysLT_1$ in the knockout.

Adult *Cysltr2* knockout mice show no retinal vascular phenotype compared with wild types (37). In agreement, preliminary analysis of isolectin-stained retinal flat mounts from P8 *Cysltr1* or *Cysltr2* knockout mice suggest that neither receptor alone is required for retinal developmental angiogenesis (data not shown). This supports the theory that cysteinyl leukotriene receptors exhibit functional redundancy.

Quininib acts as an orthosteric antagonist of the G protein-coupled receptors cysteinyl leukotriene receptor 1 and 2. Experimentally, we demonstrated quininib to significantly compete with the endogenous ligand LTD_4 for binding to $CysLT_1$ preferentially over $CysLT_2$. Additionally, quininib significantly attenuated reporter activity from $CysLT_1$ more than $CysLT_2$. It may be that a higher concentration of quininib is required to elicit a response through $CysLT_2$. These findings are in agreement with a medicinal chemistry report in 1992 by Zamboni *et al.* (51) who generated a series of $CysLT_1$ antagonists by structural modification of 3(-2-quinolinyl-(*E*)-ethenyl)pyridine. A compound equivalent to the free-base version of quininib generates an IC_{50} of >50 μM for competition with LTD_4 binding to guinea pig lung strips (51). The significantly lower IC_{50} of 1.4 μM for quininib reported here likely reflects that the human $CysLT_1$- or $CysLT_2$-overexpressing cells more specifically report on these receptors compared with the more heterogeneous guinea pig lung strips. Alternatively, the quininib hydrochloric salt used here may result in greater activity than the amine form. Finally, the chemical structure of quininib (molecular weight, 283.75 g/mol) extensively overlaps with a portion of the much larger, clinically approved $CysLT_1$ antagonist montelukast (Merck, MW 586.18g/mol) (32). Recently montelukast has been reported to reduce neuroinflammation in an aged rat model, acting via inhibition of a separate cysteinyl leukotriene receptor, GPR17 (56), and a fourth cysteinyl leukotriene receptor, GPR99, has been proposed (26). In genetic loss-of function models, cysteinyl leukotriene

FIGURE 6. **Quininib is anti-angiogenic in mammalian models of angiogenesis.** Investigation of the anti-angiogenic activity of quininib and montelukast, a $CysLT_1$ antagonist, in mammalian models of angiogenesis showed that quininib inhibited the formation of tubules *in vitro*, of sprouts *ex vivo*, and of blood vessels *in vivo*. *A* and *B*, in a quininib-treated human microvascular endothelial cell line (HMEC-1), 3.16 μM quininib inhibited the formation of tubules by 44% $\pm$ 9% ($p < 0.01$). *A*, the number of tubules qualitatively in a brightfield image (*top panel*) and stained with Calcein AM (*bottom panel*, *green*, a vital dye to show cell viability). *B*, quantification of total tubule length ($n = 3$ independent replicates; *, $p < 0.05$; **, $p < 0.01$). *C* and *D*, in a quininib-treated *ex vivo* mouse aortic ring model, 10 μM quininib reduced sprout formation (35.9 $\pm$ 13%) comparable to 10 M montelukast (43.9 $\pm$ 15.4%), whereas vehicle control did not reduce sprout formation (0%) ($n = 3$ independent replicates with 6 aortic rings/replicate). *E* and *F*, in a drug-treated mouse model of ocular angiogenesis, the oxygen-induced retinopathy model, both 0.5, and 3 μM quininib, injected on P12, prevented the revascularization of the central retina at P17, as evidenced by a larger avascular area (spaces enclosed within the *lines*) in 0.5 μM (25.5%, $p < 0.0001$) and 3 μM (23.9%, $p < 0.001$) quininib-treated eyes compared with vehicle control (16% avascular area). 0.5 μM montelukast-treated eyes did not show a statistically significant increase in avascular area compared with the control. Shown are qualitative representative isolectin-stained flat-mount retina images of vehicle control, 0.5 μM quininib, and 0.5 μM montelukast (*E*) and a scatter dot plot with *lines* denoting mean $\pm$ S.E. (*F*). Statistics were performed using one-way ANOVA (with Dunnett's post hoc test; **, $p < 0.01$; ***, $p < 0.001$), and $n >$ 18 mice across three or more independent OIR experiments (vehicle control, quininib 0.5 μM and 3 μM) and four or five mice in one OIR experiment (0.5 μM montelukast and 0.05 μM quininib). A subset ($n = 8$–9) of the quininib- and vehicle-treated OIR samples was further analyzed for percentage neovascular area (*G*) and vascular density (*H* and *I*). *G*, scatter dot plot showing the amount of retinal neovascularization as a percentage of total retinal area measured from a 0.58 mm^2 area for each quadrant. Drug treatment with 3 μM quininib resulted in an increase in the area of neovascularization (25.8%) compared with vehicle (12.8%). Statistics were performed using one-way ANOVA (with Dunnett's post hoc test). **, $p < 0.01$. *H*, a subset ($n = 8$–9) of the quininib- and vehicle-treated OIR samples was further analyzed for vascular density (*H* and *I*). A single quadrant was selected per sample, and the relative vascular staining (isolectin) was quantified as a percentage of the entire quadrant every 4 μm from 0–84 μm (representative data from a single quadrant are graphed in *H*). The maximum staining in all groups was seen in the superficial retina ~20 μm from the vitreous. Vascular density was highest in the 3 μM quininib-treated sample and lowest in 0.5 μM quininib-treated animals when compared with vehicle. Representative quantitative data (*H*) and representative qualitative data from a z-slice 24 μm from the vitreous (*I*) is shown. *, $p < 0.05$; **, $p < 0.01$.

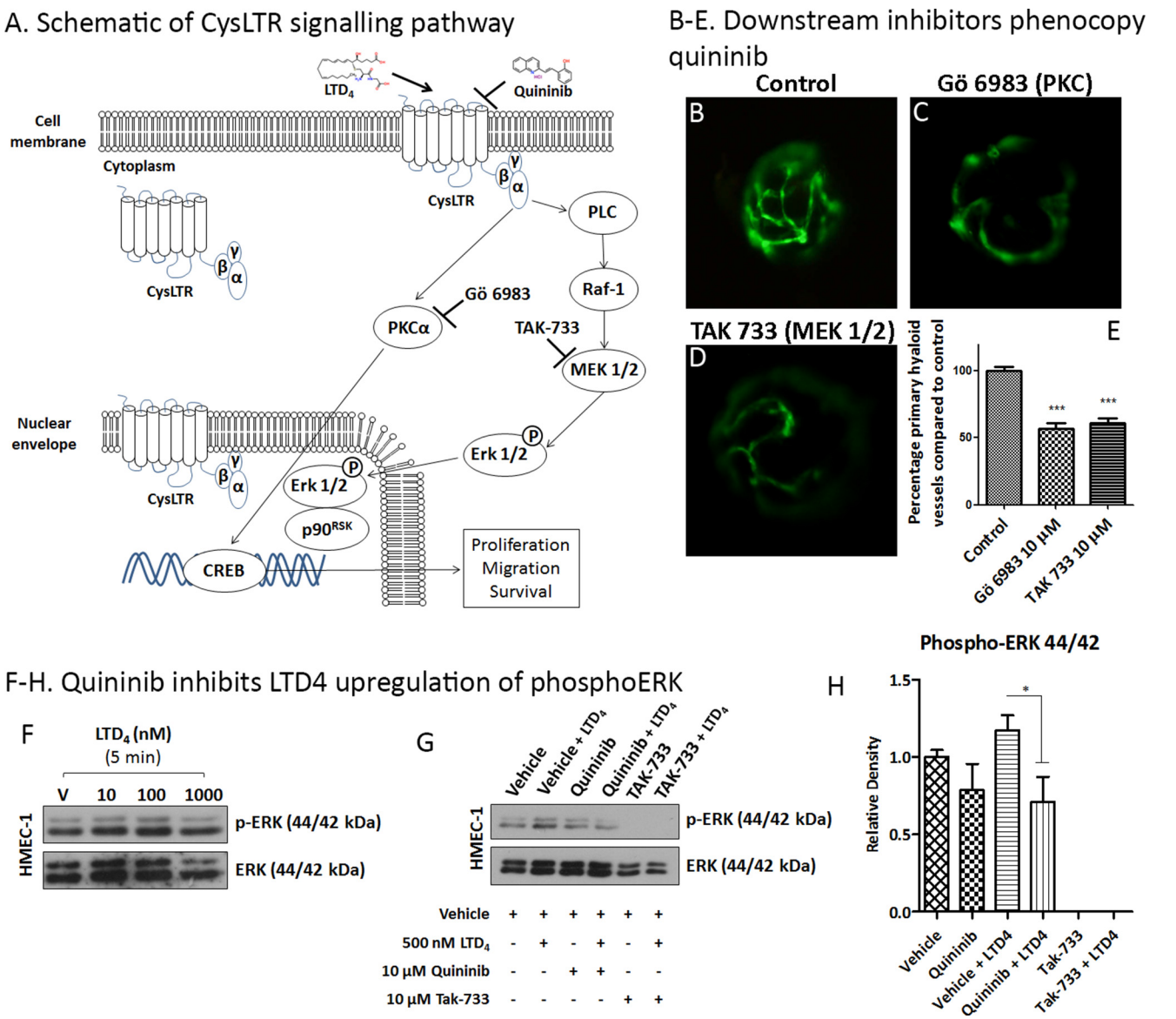

FIGURE 7. **Quininib inhibits cysteinyl leukotriene receptor signaling pathways.** Investigation of signaling pathways reported to be downstream of cysteinyl leukotriene receptors (*A*) showed that known pharmacological inhibitors of this signaling pathway phenocopy quininib and that quininib can inhibit leukotriene D4 up-regulation of phospho-ERK. *A*, schematic (modified from Savari *et al.* (69)) showing the signaling pathway downstream of CysLTR (shown in cell membrane, cytoplasmic, and nuclear localization). *B*—*E*, drug treatment of transgenic Tg[*fli1*:EGFP] zebrafish from 2–5 dpf with 10 μM pan-PKC inhibitor Gö 6983 (*C*) or 10 μM MEK 1/2 inhibitor TAK-733 (*D*) inhibited the development of primary hyaloid vessels (*green*) compared with vehicle control (0.1% DMSO, *B*) in a significant manner (*E*, $n = 20$–30 larvae/compound, ***, $p < 0.001$). *F*, treatment of endothelial HMEC-1 cells with 10, 100, and 1000 nM LTD_4 for 5 min up-regulated downstream ERK phosphorylation. *G*, pretreatment of HMEC-1 cells for 30 min with vehicle (*V*) control (0.1% DMSO), quininib, or the MEK 1/2 inhibitor TAK-733 followed by a 5-min stimulation with 500 nM LTD_4 or vehicle (0.25% ethanol) showed that quininib and TAK-733 inhibited LTD_4 induced phospho-ERK up-regulation. Shown is a representative Western blotting analysis. *H*, densitometry analysis of phospho-ERK expression normalized to ERK expression showing that quininib inhibited LTD_4-induced phospho-ERK up-regulation (a decrease of 46% in phospho-ERK expression in vehicle *versus* quininib LTD_4-stimulated HMEC-1 cells, $n = 4$ repetitions). One-way ANOVA showed that quininib inhibited LTD_4-induced phospho-ERK up-regulation in a statistically significant manner. *, $p < 0.05$).

receptors demonstrate cognate compensatory up-regulation (37, 39, 57). Thus, there are exciting future opportunities to decipher the cysLT receptors exhibiting co-regulatory expression to understand the underlying control mechanisms and to determine the combinations of cysLT receptors that regulate physiological phenotypes.

Cysteinyl leukotrienes have been reported previously to up-regulate ERK phosphorylation (38, 39). Here we show that drug treatment with quininib inhibits LTD_4-induced phospho-ERK up-regulation, which is completely blocked by the more downstream MEK 1/2 inhibitor TAK-733. TAK-733 and the broad-spectrum PKC inhibitor Gö 6983 phenocopy the effects of quininib on developing hyaloid vessels in zebrafish.

On the basis of a virtual drug screen, the quininib E-isomer was reported in 2008 to inhibit endothelin-converting enzyme 2 (ECE-2) (49). This target is unlikely to mediate the anti-angiogenic activity of quininib because alternative endothelin receptor antagonists do not phenocopy quininib (data not shown). In addition, recently Gupta *et al.* (50) reported that the quininib Z-isomer more potently inhibits ECE-2 than the E-isomer, which does not correlate with our finding of greater anti-

angiogenic activity of the E-isomer (50). Also of note is that quininib does not directly inhibit the activity of any VEGF receptor. VEGF, particularly in the eye, is a key target to treat ocular neovascularization using humanized antibodies (*e.g.* Avastin®, Lucentis®) or soluble decoy receptors (Eylea®), and many small-molecule VEGF receptor inhibitors are available (*e.g.* the tyrosine kinase inhibitors AL 39324, PTK787, and Tg 100801; reviewed in Ref. 58). Thus, the distinct cysteinyl leukotriene pathway-mediated anti-angiogenic mechanism of action of quininib offers potential for additive effects with anti-VEGFs or alternative therapeutic targets for patients non-responsive to current anti-VEGFs (15).

Although this is the first report demonstrating a significant anti-angiogenic effect of $CysLT_1$ antagonists on ocular angiogenesis, accumulating evidence confirms a key role for cysteinyl leukotrienes in angiogenesis. For example, the cysteinyl leukotrienes LTD_4 and LTC_4 stimulate angiogenesis in endothelial cells (59, 60). Of particular relevance, the $CysLT_1$ antagonist montelukast, but not the $CysLT_2$ antagonist BayCysLT2, blocks the LTD_4-induced migratory phenotype of the human endothelial cell line EA.hy926 (61). Similarly, montelukast, but not BayCysLT2, inhibits basal microvessel outgrowth from rat thoracic aortic rings, and both drugs inhibit an LTD_4-induced model of aortic ring angiogenesis (62). *In vivo*, Savari *et al.* (63) recently reported $CysLT_1$ receptor antagonists to reduce tumor angiogenesis in a mouse xenograft model of colorectal cancer, and this was concomitant with reduced tumor VEGF levels. Interestingly, the recognized anti-asthmatic effect of montelukast is modulated by VEGF polymorphisms, and montelukast has been postulated to attenuate airway inflammation by reducing VEGF expression (64, 65). Focusing on the eye, Barajas-Espinosa *et al.* (37), in defining a role for $CysLT_2$ in retinal permeability and neovascularization, also demonstrated expression of $CysLT_1$ in the retina, which is significantly increased upon knockout of *Cysltr2*. Here we demonstrate that the zebrafish *cysltr1* and *cysltr2* genes are expressed in the eye during hyaloid vasculature development and that the $CysLT_1$ antagonist quininib can attenuate ocular angiogenesis. Intriguingly, quininib is significantly more potent than montelukast at inhibiting angiogenesis in the eye. Pharmacokinetic reasons potentially explain these differences. Quininib is significantly smaller than montelukast, which may facilitate greater absorption into the zebrafish eye and greater penetration across the mouse retinal layers, resulting in enhanced bioavailability and efficacy. Additionally, montelukast is known to undergo light-induced isomerization, which produces structurally related but inactive products (66).

In summary, we demonstrate a novel role for cysteinyl leukotriene receptor antagonists in attenuating ocular angiogenesis. Cysteinyl leukotrienes are proinflammatory agents that increase vascular permeability (26, 29) through receptor-mediated activation of phospholipase C, phosphoinositide-3-kinase, and/or extracellular signal-related kinases (29, 67, 68). This increased permeability can increase extravasation of proangiogenic factors that can remodel the extracellular environment and promote growth of new vessels. CysLTs provide a novel pathway from which to enhance our understanding of developmental angiogenesis and a novel therapeutic target in angiogenesis-driven disease.

Author Contributions—A. L. R. conducted validation, visual behavior, analogue, and time-course experiments in zebrafish; safety and efficacy experiments in mice; and target profiling analyses, analyzed and interpreted the results, and wrote the paper with Y. A. and B. N. K. Y. A. and N. W. conducted the initial drug discovery and safety experiments in zebrafish and analyzed the results. T. S. performed zebrafish behavioral assays, expression analyses, and downstream cysLT signaling experiments and analyzed the results. C. B. performed HMEC-1 cell viability studies and the *in vitro* tubule formation assay. C. K. performed the target profiling analysis and helped with mouse OIR experiments. A. J. S. performed screening of downstream cysteinyl leukotriene inhibitors in zebrafish. C. M. and V. H. Y. W. performed a subset of the mouse OIR experiments, analyzed the results, and assisted with the interpretation of results. O. G. performed the mouse aortic ring experiments. S. M. performed the ARPE-19 cell viability studies. J. O. and A. S. provided animal models. G. G. performed analysis of OIR mouse retinas. A. W. S. provided animal models and assisted with analysis and interpretation of the results. B. N. K. conceived the idea for the project, assisted with analysis and interpretation of the results, and wrote the paper with A. L. R. and Y. A.

Acknowledgments—We thank the Conway Institute Imaging Core Technology, especially Dimitri Scholz, for assistance with montaging and Tiina O'Neill and Kasia Welzel for assistance with embedding and sectioning of samples; Pat Guiry for help with interpreting chemical structures; Ken O'Halloran for access to hyperoxia equipment; and Adrian Murphy, Jacintha O'Sullivan, Nils Ohnesorge, and Oliver Blacque for discussions and comments on the manuscript.

References

1. Fruttiger, M. (2007) Development of the retinal vasculature. *Angiogenesis* **10,** 77–88
2. Cheung, N., Mitchell, P., and Wong, T. Y. (2010) Diabetic retinopathy. *Lancet* **376,** 124–136
3. Jager, R. D., Mieler, W. F., and Miller, J. W. (2008) Age-related macular degeneration. *N. Engl. J. Med.* **358,** 2606–2617
4. Hellström, A., Smith, L. E., and Dammann, O. (2013) Retinopathy of prematurity. *Lancet* **382,** 1445–1457
5. Rehak, M., and Wiedemann, P. (2010) Retinal vein thrombosis: pathogenesis and management. *J. Thromb. Haemost.* **8,** 1886–1894
6. Gariano, R. F., and Gardner, T. W. (2005) Retinal angiogenesis in development and disease. *Nature* **438,** 960–966
7. Alvarez, Y., Astudillo, O., Jensen, L., Reynolds, A. L., Waghorne, N., Brazil, D. P., Cao, Y., O'Connor, J. J., and Kennedy, B. (2009) Selective inhibition of retinal angiogenesis by targeting PI3 kinase. *PLoS ONE* **4,** e7867
8. Kitambi, S. S., McCulloch, K. J., Peterson, R. T., and Malicki, J. J. (2009) Small molecule screen for compounds that affect vascular development in the zebrafish retina. *Mech. Dev.* **126,** 464–477
9. Folkman, J. (1997) in *Regulation of Angiogenesis* (Goldberg, I., and Rosen, E., eds.) pp. 1–8, Birkhäuser, Basel, Switzerland
10. Frost & Sullivan (June 7, 2011) *Analysis of the US Retinal Therapeutics Market: Improvements in Administration and Efficacy Drive Growth*, Frost & Sullivan Report NC77–52
11. Frost & Sullivan (July 3, 2010) *European Ophthalmic Pharmaceuticals Market*, Frost & Sullivan Report M4AC-52
12. CATT Research Group, Martin, D. F., Maguire, M. G., Ying, G. S., Grunwald, J. E., Fine, S. L., and Jaffe, G. J. (2011) Ranibizumab and bevacizumab for neovascular age-related macular degeneration. *N. Engl. J. Med.* **364,** 1897–1908

13. Heier, J. S., Brown, D. M., Chong, V., Korobelnik, J.-F., Kaiser, P. K., Nguyen, Q. D., Kirchhof, B., Ho, A., Ogura, Y., Yancopoulos, G. D., Stahl, N., Vitti, R., Berliner, A. J., Soo, Y., Anderesi, M., Groetzbach, G., Sommerauer, B., Sandbrink, R., Simader, C., Schmidt-Erfurth, U., and VIEW 1 and VIEW 2 Study Groups. (2012) Intravitreal aflibercept (VEGF trap-eye) in wet age-related macular degeneration. *Ophthalmology* **119,** 2537–2548
14. Rosenfeld, P. J., Brown, D. M., Heier, J. S., Boyer, D. S., Kaiser, P. K., Chung, C. Y., Kim, R. Y., and MARINA Study Group (2006) Ranibizumab for neovascular age-related macular degeneration. *N. Engl. J. Med.* **355,** 1419–1431
15. Rofagha, S., Bhisitkul, R. B., Boyer, D. S., Sadda, S. R., Zhang, K., and SEVEN-UP Study Group (2013) Seven-year outcomes in ranibizumab-treated patients in ANCHOR, MARINA, and HORIZON: a multicenter cohort study (SEVEN-UP). *Ophthalmology* **120,** 2292–2299
16. Diabetic Retinopathy Clinical Research Network, Elman, M. J., Qin, H., Aiello, L. P., Beck, R. W., Bressler, N. M., Ferris, F. L., 3rd, Glassman, A. R., Maturi, R. K., and Melia, M. (2012) Intravitreal ranibizumab for diabetic macular edema with prompt vs. deferred laser treatment: 3-year randomized trial results. *Ophthalmology* **119,** 2312–2318
17. Wangsa-Wirawan, N. D., and Linsenmeier, R. A. (2003) Retinal oxygen: fundamental and clinical aspects. *Arch. Ophthalmol.* **121,** 547–557
18. Saint-Geniez, M., and D'Amore, P. (2004) Development and pathology of the hyaloid, choroidal and retinal vasculature. *Int. J. Dev. Biol.* **48,** 1045–1058
19. Fruttiger, M. (2002) Development of the mouse retinal vasculature: angiogenesis versus vasculogenesis. *Invest. Ophthalmol. Vis. Sci.* **43,** 522–527
20. Shastry, B. S. (2009) Persistent hyperplastic primary vitreous: congenital malformation of the eye. *Clin. Exp. Ophthalmol.* **37,** 884–890
21. Alvarez, Y., Cederlund, M. L., Cottell, D. C., Bill, B. R., Ekker, S. C., Torres-Vazquez, J., Weinstein, B. M., Hyde, D. R., Vihtelic, T. S., and Kennedy, B. N. (2007) Genetic determinants of hyaloid and retinal vasculature in zebrafish. *BMC Dev. Biol.* **7,** 114
22. Hartsock, A., Lee, C., Arnold, V., and Gross, J. M. (2014) *In vivo* analysis of hyaloid vasculature morphogenesis in zebrafish: a role for the lens in maturation and maintenance of the hyaloid. *Dev. Biol.* **394,** 327–339
23. Kalén, M., Wallgard, E., Asker, N., Nasevicius, A., Athley, E., Billgren, E., Larson, J. D., Wadman, S. A., Norseng, E., Clark, K. J., He, L., Karlsson-Lindahl, L., Häger, A.-K., Weber, H., Augustin, H., Samuelsson, T., Kemmet, C. K., Utesch, C. M., Essner, J. J., Hackett, P. B., and Hellström, M. (2009) Combination of reverse and chemical genetic screens reveals angiogenesis inhibitors and targets. *Chem. Biol.* **16,** 432–441
24. Peterson, R. T., Link, B. A., Dowling, J. E., and Schreiber, S. L. (2000) Small molecule developmental screens reveal the logic and timing of vertebrate development. *Proc. Natl. Acad. Sci. U.S.A.* **97,** 12965–12969
25. Rennekamp, A. J., and Peterson, R. T. (2015) 15 years of zebrafish chemical screening. *Curr. Opin. Chem. Biol.* **24,** 58–70
26. Kanaoka, Y., Maekawa, A., and Austen, K. F. (2013) Identification of GPR99 protein as a potential third cysteinyl leukotriene receptor with a preference for leukotriene E4 ligand. *J. Biol. Chem.* **288,** 10967–10972
27. Singh, R. K., Gupta, S., Dastidar, S., and Ray, A. (2010) Cysteinyl leukotrienes and their receptors: molecular and functional characteristics. *Pharmacology* **85,** 336–349
28. Kanaoka, Y., and Boyce, J. A. (2004) Cysteinyl leukotrienes and their receptors: cellular distribution and function in immune and inflammatory responses. *J. Immunol.* **173,** 1503–1510
29. Bäck, M., Powell, W. S., Dahlén, S. E., Drazen, J. M., Evans, J. F., Serhan, C. N., Shimizu, T., Yokomizo, T., and Rovati, G. E. (2014) Update on leukotriene, lipoxin and oxoeicosanoid receptors: IUPHAR Review 7. *Br. J. Pharmacol.* **171,** 3551–3574
30. Ciana, P., Fumagalli, M., Trincavelli, M. L., Verderio, C., Rosa, P., Lecca, D., Ferrario, S., Parravicini, C., Capra, V., Gelosa, P., Guerrini, U., Belcredito, S., Cimino, M., Sironi, L., Tremoli, E., Rovati, G. E., Martini, C., and Abbracchio, M. P. (2006) The orphan receptor GPR17 identified as a new dual uracil nucleotides/cysteinyl-leukotrienes receptor. *EMBO J.* **25,** 4615–4627
31. Meltzer, E. O., Malmstrom, K., Lu, S., Prenner, B. M., Wei, L. X., Weinstein, S. F., Wolfe, J. D., and Reiss, T. F. (2000) Concomitant montelukast and loratadine as treatment for seasonal allergic rhinitis: a randomized, placebo-controlled clinical trial. *J. Allergy Clin. Immunol.* **105,** 917–922
32. Reiss, T. F., Altman, L. C., Chervinsky, P., Bewtra, A., Stricker, W. E., Noonan, G. P., Kundu, S., and Zhang, J. (1996) Effects of montelukast (MK-0476), a new potent cysteinyl leukotriene (LTD4) receptor antagonist, in patients with chronic asthma. *J. Allergy Clin. Immunol.* **98,** 528–534
33. Kyritsis, N., Kizil, C., Zocher, S., Kroehne, V., Kaslin, J., Freudenreich, D., Iltzsche, A., and Brand, M. (2012) Acute inflammation initiates the regenerative response in the adult zebrafish brain. *Science* **338,** 1353–1356
34. Qian, X.-D., Wei, E.-Q., Zhang, L., Sheng, W.-W., Wang, M.-L., Zhang, W.-P., and Chen, Z. (2006) Pranlukast, a cysteinyl leukotriene receptor 1 antagonist, protects mice against brain cold injury. *Eur. J. Pharmacol.* **549,** 35–40
35. Wang, X. Y., Tang, S. S., Hu, M., Long, Y., Li, Y. Q., Liao, M. X., Ji, H., and Hong, H. (2013) Leukotriene D4 induces amyloid-β generation via CysLT1R-mediated NF-κB pathways in primary neurons. *Neurochem. Int.* **62,** 340–347
36. Kanaoka, Y., and Boyce, J. A. (2014) Cysteinyl leukotrienes and their receptors: emerging concepts. *Allergy Asthma Immunol. Res.* **6,** 288–295
37. Barajas-Espinosa, A., Ni, N. C., Yan, D., Zarini, S., Murphy, R. C., and Funk, C. D. (2012) The cysteinyl leukotriene 2 receptor mediates retinal edema and pathological neovascularization in a murine model of oxygen-induced retinopathy. *FASEB J.* **26,** 1100–1109
38. Duah, E., Adapala, R. K., Al-Azzam, N., Kondeti, V., Gombedza, F., Thodeti, C. K., and Paruchuri, S. (2013) Cysteinyl leukotrienes regulate endothelial cell inflammatory and proliferative signals through CysLT(2) and CysLT(1) receptors. *Sci. Rep.* **3,** 3274
39. Jiang, Y., Borrelli, L. A., Kanaoka, Y., Bacskai, B. J., and Boyce, J. A. (2007) CysLT(2) receptors interact with CysLT(1) receptors and down-modulate cysteinyl leukotriene-dependent mitogenic responses of mast cells. *Blood* **110,** 3263–3270
40. Lipinski, C., Lombardo, F., Dominy, B., and Feeney, P. (2001) Experimental and computational approaches to estimate solubility and permeability in drug discovery and development settings. *Adv. Drug Deliv. Rev.* **23,** 3–26
41. Lawson, N. D., and Weinstein, B. M. (2002) *In vivo* imaging of embryonic vascular development using transgenic zebrafish. *Dev. Biol.* **248,** 307–318
42. Brockerhoff, S. (2006) Measuring the optokinetic response of zebrafish larvae. *Nat. Protoc.* **1,** 2448–2451
43. Sasore, T., and Kennedy, B. (2014) Deciphering combinations of PI3K/AKT/mTOR pathway drugs augmenting anti-angiogenic efficacy *in vivo*. *PLoS ONE* **9,** e105280
44. Baker, M., Robinson, S. D., Lechertier, T., Barber, P. R., Tavora, B., D'Amico, G., Jones, D. T., Vojnovic, B., and Hodivala-Dilke, K. (2012) Use of the mouse aortic ring assay to study angiogenesis. *Nat. Protoc.* **7,** 89–104
45. Connor, K. M., Krah, N. M., Dennison, R. J., Aderman, C. M., Chen, J., Guerin, K. I., Sapieha, P., Stahl, A., Willett, K. L., and Smith, L. E. (2009) Quantification of oxygen-induced retinopathy in the mouse: a model of vessel loss, vessel regrowth and pathological angiogenesis. *Nat. Protoc.* **4,** 1565–1573
46. Smith, L. E., Wesolowski, E., McLellan, A., Kostyk, S. K., D'Amato, R., Sullivan, R., and D'Amore, P. A. (1994) Oxygen-induced retinopathy in the mouse. *Invest. Ophthalmol. Vis. Sci.* **35,** 101–111
47. Gardiner, T. A., Gibson, D. S., de Gooyer, T. E., de la Cruz, V. F., McDonald, D. M., and Stitt, A. W. (2005) Inhibition of tumor necrosis factor-α improves physiological angiogenesis and reduces pathological neovascularization in ischemic retinopathy. *Am. J. Pathol.* **166,** 637–644
48. Sidman, R. L., Li, J., Lawrence, M., Hu, W., Musso, G. F., Giordano, R. J., Cardó-Vila, M., Pasqualini, R., and Arap, W. (2015) The peptidomimetic Vasotide targets two retinal VEGF receptors and reduces pathological angiogenesis in murine and nonhuman primate models of retinal disease. *Sci. Transl. Med.* **7,** 309ra165–309ra165
49. Gagnidze, K., Sachchidanand, Rozenfeld, R., Mezei, M., Zhou, M.-M., and Devi, L. A. (2008) Homology modeling and site-directed mutagenesis to identify selective inhibitors of endothelin-converting enzyme-2. *J. Med. Chem.* **51,** 3378–3387

50. Gupta, A., Gomes, I., Wardman, J., and Devi, L. A. (2014) Opioid receptor function is regulated by post-endocytic peptide processing. *J. Biol. Chem.* **289,** 19613–19626
51. Zamboni, R., Belley, M., Champion, E., Charette, L., DeHaven, R., Frenette, R., Gauthier, J. Y., Jones, T. R., Leger, S., and Masson, P. (1992) Development of a novel series of styrylquinoline compounds as high-affinity leukotriene D4 receptor antagonists: synthetic and structure-activity studies leading to the discovery of (+−)-3-[[[3-[2-(7-chloro-2-quinolinyl)-(E)-ethenyl]phenyl][[3-(dimethylamino)-3-oxopropyl]thio]methyl]thio]propionic acid. *J. Med. Chem.* **35,** 3832–3844
52. Lorusso, P. M., Boerner, S. A., and Hunsberger, S. (2011) Clinical development of vascular disrupting agents: what lessons can we learn from ASA404? *J. Clin. Oncol.* **29,** 2952–2955
53. Dhakal, S., Stevens, C., Weiss, O., Inbal, A., and Stenkamp, D. (2013) Role of the early ocular vasculature in regulation of retinal neurogenesis. *Invest. Ophthalmol. Vis. Sci.* **54,** Abstr. 5145
54. Dhakal, S., Stevens, C. B., Sebbagh, M., Weiss, O., Frey, R. A., Adamson, S., Shelden, E. A., Inbal, A., and Stenkamp, D. L. (2015) Abnormal retinal development in Cloche mutant zebrafish. *Dev. Dyn.* **244,** 1439–1455
55. Stahl, A., Connor, K. M., Sapieha, P., Chen, J., Dennison, R. J., Krah, N. M., Seaward, M. R., Willett, K. L., Aderman, C. M., Guerin, K. I., Hua, J., Löfqvist, C., Hellström, A., and Smith, L. E. (2010) The mouse retina as an angiogenesis model. *Invest. Ophthalmol. Vis. Sci.* **51,** 2813–2826
56. Marschallinger, J., Schaffner, I., Klein, B., Gelfert, R., Rivera, F. J., Illes, S., Grassner, L., Janssen, M., Rotheneichner, P., Schmuckermair, C., Coras, R., Boccazzi, M., Chishty, M., Lagler, F. B., Renic, M., Bauer, H.-C., Singewald, N., Blumcke, I., Bogdahn, U., Couillard-Despres, S., Lie, D. C., Abbracchio, M. P., and Aigner, L. (2015) Structural and functional rejuvenation of the aged brain by an approved anti-asthmatic drug. *Nat. Commun.* **6,** 8466
57. Maekawa, A., Kanaoka, Y., Xing, W., and Austen, K. F. (2008) Functional recognition of a distinct receptor preferential for leukotriene E(4) in mice lacking the cysteinyl leukotriene 1 and 2 receptors. *Proc. Natl. Acad. Sci. U.S.A.* **105,** 16695–16700
58. Reynolds, A. L., Kent, D., and Kennedy, B. N. (2014) Ocular neovascularisation: current and emerging therapies. *Adv. Exp. Med. Biol.* **801,** 797–804
59. Tsopanoglou, N. E., Pipili-Synetos, E., and Maragoudakis, M. E. (1994) Leukotrienes C4 and D4 promote angiogenesis via a receptor-mediated interaction. *Eur. J. Pharmacol.* **258,** 151–154
60. Kanayasu, T., Nakao-Hayashi, J., Asuwa, N., Morita, I., Ishii, T., Ito, H., and Murota, S. (1989) Leukotriene C4 stimulates angiogenesis in bovine carotid artery endothelial cells *in vitro*. *Biochem. Biophys. Res. Commun.* **159,** 572–578
61. Yuan, Y.-M., Fang, S.-H., Qian, X.-D., Liu, L.-Y., Xu, L.-H., Shi, W.-Z., Zhang, L.-H., Lu, Y.-B., Zhang, W.-P., and Wei, E.-Q. (2009) Leukotriene D4 stimulates the migration but not proliferation of endothelial cells mediated by the cysteinyl leukotriene CysLT1 receptor via the extracellular signal-regulated kinase pathway. *J. Pharmacol. Sci.* **109,** 285–292
62. Xu, L., Zhang, L., Liu, L., Fang, S., Lu, Y., Wei, E., and Zhang, W. (2010) Involvement of cysteinyl leukotriene receptors in angiogenesis in rat thoracic aortic rings. *Pharmazie* **65,** 750–754
63. Savari, S., Liu, M., Zhang, Y., Sime, W., and Sjölander, A. (2013) CysLT1R antagonists inhibit tumor growth in a xenograft model of colon cancer. *PLoS ONE* **8,** e73466
64. Balantic, M., Rijavec, M., Skerbinjek Kavalar, M., Suskovic, S., Silar, M., Kosnik, M., and Korosec, P. (2012) Asthma treatment outcome in children is associated with vascular endothelial growth factor A (VEGFA) polymorphisms. *Mol. Diagn. Ther.* **16,** 173–180
65. Lee, K. S., Kim, S. R., Park, H. S., Jin, G. Y., and Lee, Y. C. (2004) Cysteinyl leukotriene receptor antagonist regulates vascular permeability by reducing vascular endothelial growth factor expression. *J. Allergy Clin. Immunol.* **114,** 1093–1099
66. Smith, G. A., Rawls, C. M., and Kunka, R. L. (2004) An automated method for the determination of montelukast in human plasma using dual-column HPLC analysis and peak height summation of the parent compound and its photodegradation product. *Pharm. Res.* **21,** 1539–1544
67. Kim, M. H., Lee, Y. J., Kim, M. O., Kim, J. S., and Han, H. J. (2010) Effect of leukotriene D4 on mouse embryonic stem cell migration and proliferation: involvement of PI3K/Akt as well as GSK-3β/β-catenin signaling pathways. *J. Cell Biochem.* **111,** 686–698
68. Salim, T., Sand-Dejmek, J., and Sjölander, A. (2014) The inflammatory mediator leukotriene D4 induces subcellular β-catenin translocation and migration of colon cancer cells. *Exp. Cell Res.* **321,** 255–266
69. Savari, S., Vinnakota, K., Zhang, Y., and Sjölander, A. (2014) Cysteinyl leukotrienes and their receptors: bridging inflammation and colorectal cancer. *World J. Gastroenterol.* **20,** 968–977